Supplemental Information

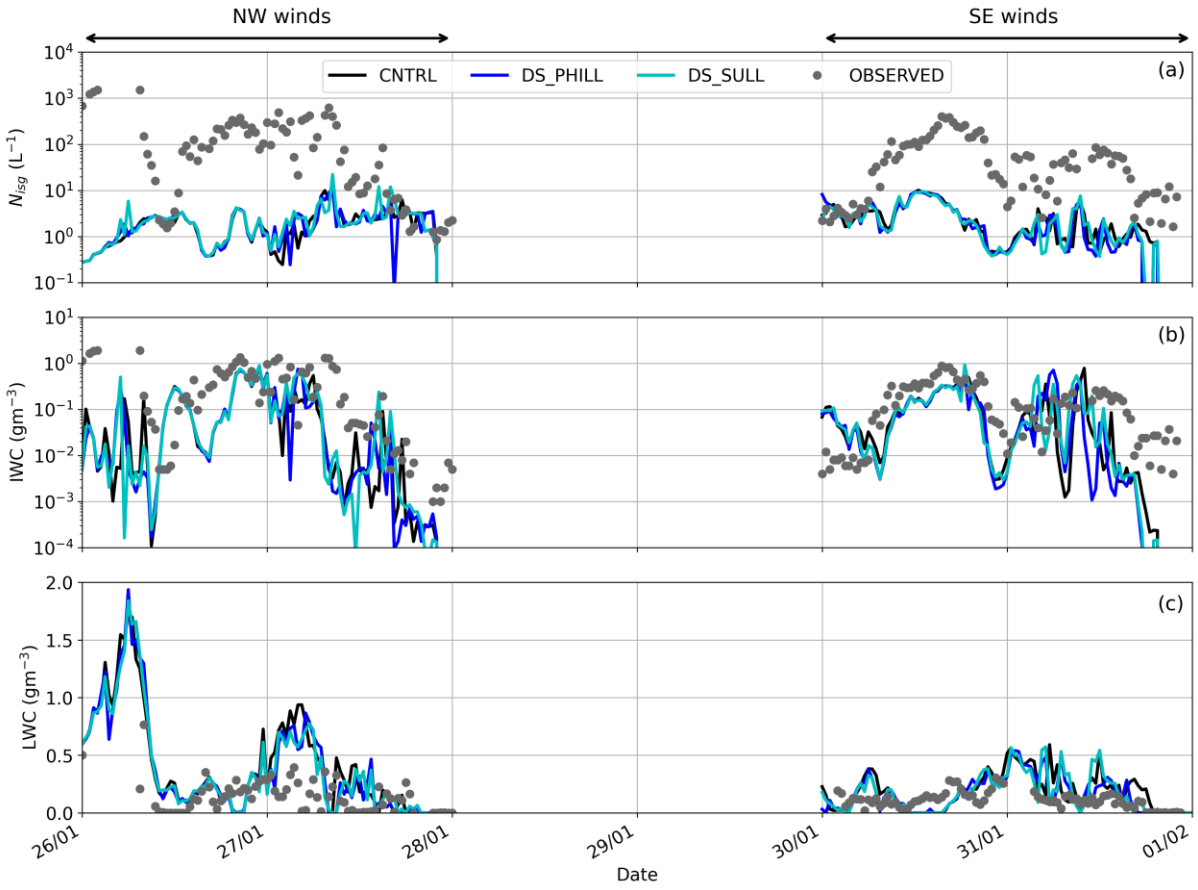

Figure S1. Timeseries of (a) total ice number concentrations (N_{isg}; cloud ice + snow + graupel), (b) ice water content (IWC) and (c) liquid water content (LWC), predicted by the control simulation of WRF (CNTRL; black line) and the two sensitivity simulations including a description of the droplet shattering (DS) process, parameterized following Phillips et al. (2018) (DS_PHILL; blue line) and Sullivan et al. (2018) (DS_SULL; cyan line). The grey dots in (a), (b) and (c) represent the respective measurements of N_{isg}, IWC and LWC, taken between 26 January and 1 February 2014 at Jungfraujoch (JFJ) at an altitude of 3580 m above sea level (a.s.l.). Each day starts at 00 UTC. Note the logarithmic y-axes in panels a and b.

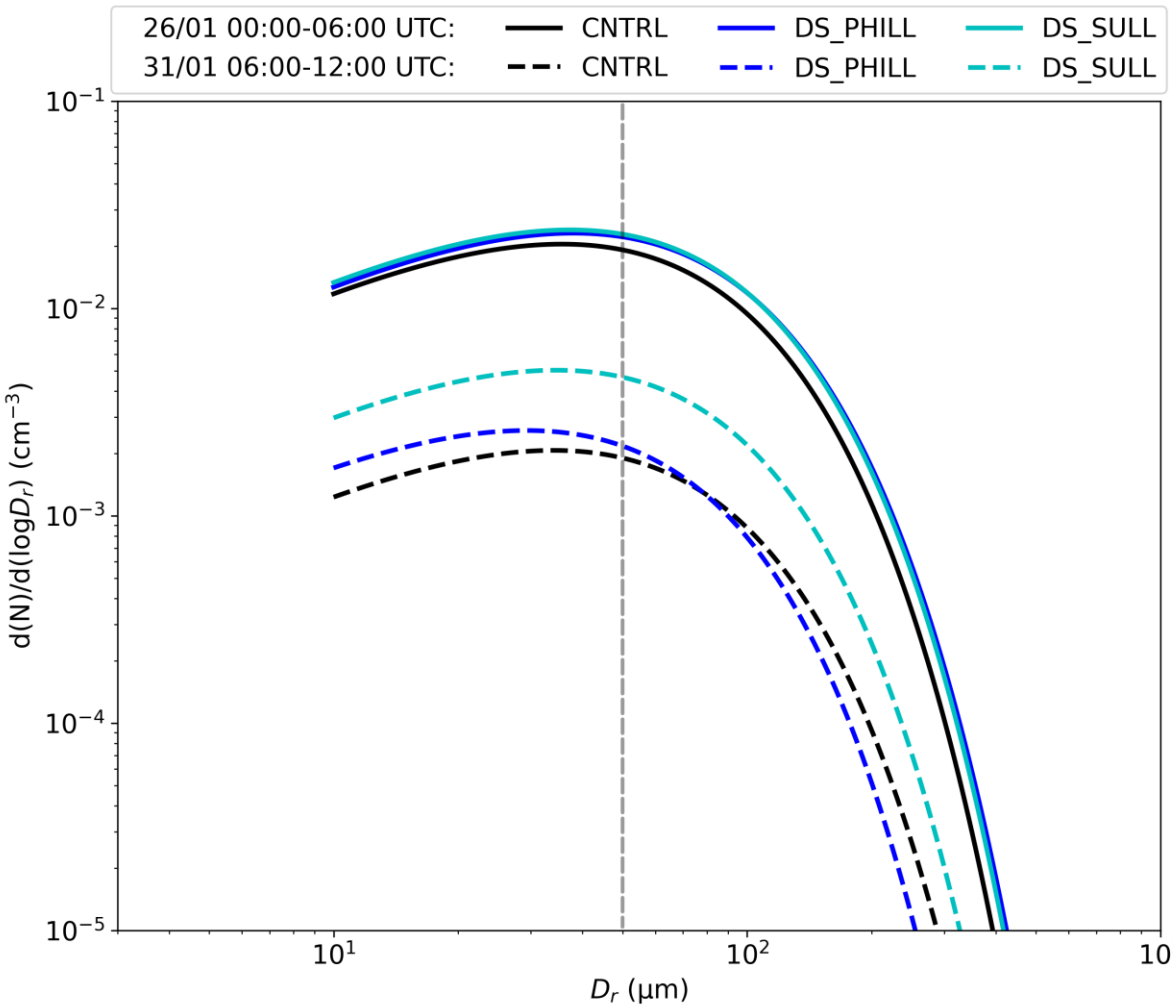

Figure S2. Size distribution of raindrops predicted by the CNTRL, DS_PHILL and DS_SULL simulations. The size distributions were averaged between 00:00 and 06:00 UTC on 26 January (solid line) and between 06:00 and 12:00 UTC on 31 January (dashed line). The vertical dashed grey line indicates the threshold size of 50 μm, which is required for DS to be activated.

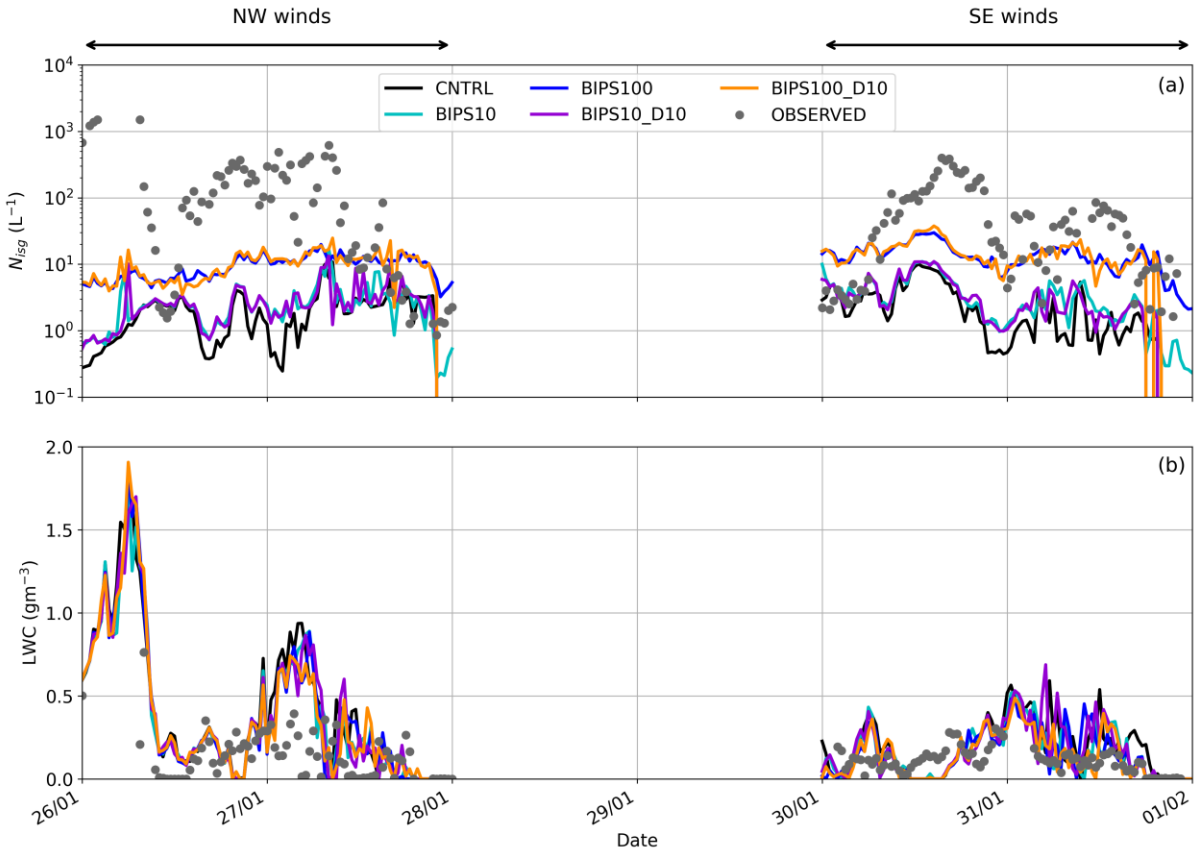

Figure S3. Time series of (a) total N_{isg} and (b) LWC, predicted between 26 January and 1 February 2014 by the sensitivity simulations including a source of ice crystals in the first atmospheric level to represent the microphysical effect of blowing snow ice particles (BIPS). We consider spherical particles with sizes of 10 µm (suffix D10) and 100 µm. The applied concentrations are equal to 10 L^{-1} in BIPS10 (cyan line) and BIPS10_D10 (purple line), and 100 L^{-1} in BIPS100 (blue line) and BIPS100_D10 (orange line).

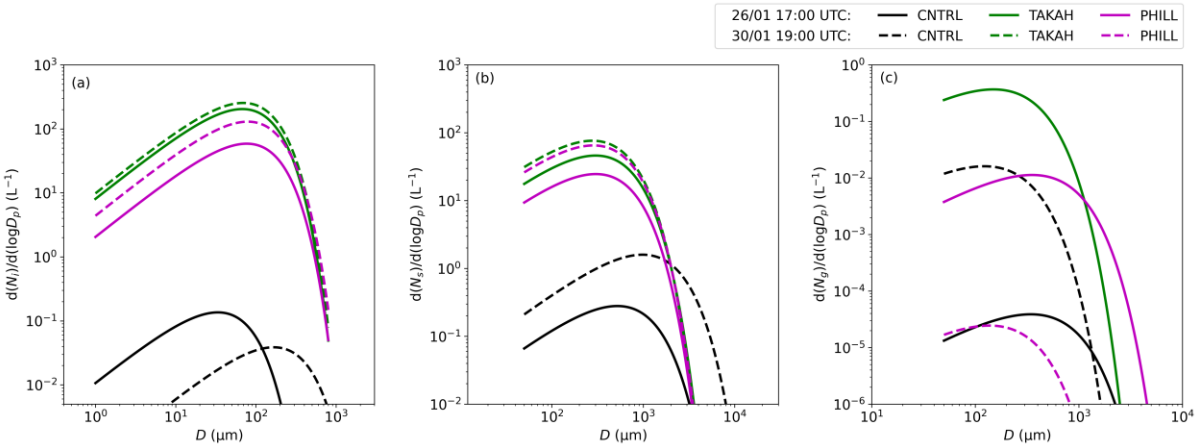

Figure S4. Size distribution of (a) cloud ice, (b) snow and (c) graupel particles, predicted by the CNTRL and the two sensitivity simulations including a description of the ice-ice collisional break-up (BR) process, parameterized following Sullivan et al. (2018) based on the laboratory findings of Takahashi et al. (1995) (TAKAH; green line) and Phillips et al. (2017) (PHILLL; magenta line). The size distributions were taken at 17:00 UTC on 26 January (solid line) and at 19:00 UTC on 30 January (dashed line). Note that TAKAH is not producing significant concentrations of graupel particles on 30 January.

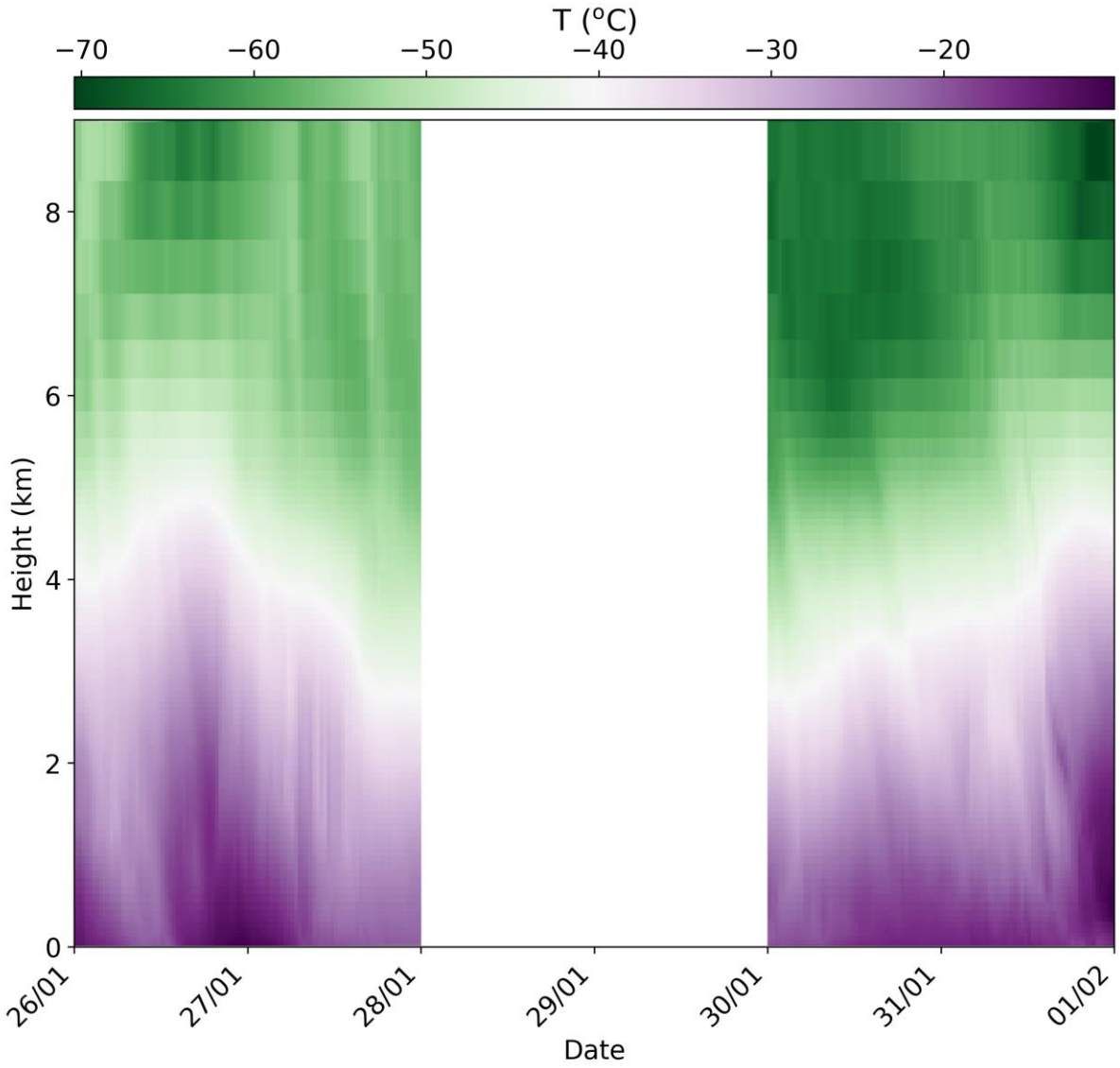

Figure S5. Height-time cross-section of temperature (T in °C) simulated from 26 January to 1 February 2014 by the CNTRL simulation at JFJ. The height is given in km above ground level (a.g.l).

TEXT S1:

During CLACE 2014, a polarimetric Doppler weather radar was deployed at Kleine Scheidegg (2061 m a.s.l; Grazioli et al., 2015). This compact system, operating at the X-band frequency is particularly well suited to provide high resolution data of the vertical structure of precipitation in complex terrains, including narrow Alpine valleys (Schneebeli et al., 2013). The radar was continuously operating with a scanning protocol of about 5 minutes including various types of scans in different directions. As the vertical structure of precipitation and its evolution in time is of particular interest for the present work, we used the data collected at various height levels along a transect in the direction of Grindelwad, roughly northeasterly with respect to the radar. Along this transect the quality of the data was only marginally affected by the clutter of the high mountains nearby and therefore a continuous depiction, in time and in space, of the vertical structure of precipitation (above the radar installation height) could be obtained.

Polarimetric data can be used to estimate the type of hydrometeors that dominates the signal within each radar resolution volume. We employed the hydrometeor classification method of Besic et al. (2018), which divides dry snowfall into three categories: crystals, when individual and relatively small crystals dominate; aggregates and rimed ice particles, including graupel and heavily rimed snow.

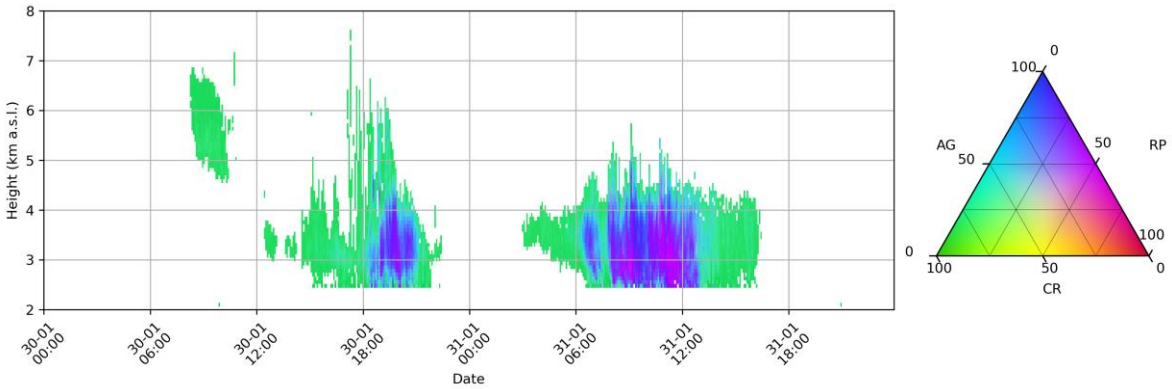

Figure S6. Radar-based hydrometeor classification between 30 and 31 January. Dry snowfall is classified into three categories: aggregates (AG), individual crystals (CR) and rimed ice particles (RI). This data should be interpreted as representative of the overall behavior along a transect of 4 km length (from 2 to 6 km distance from the radar) in the northeasterly direction. The height is given in km a.s.l.

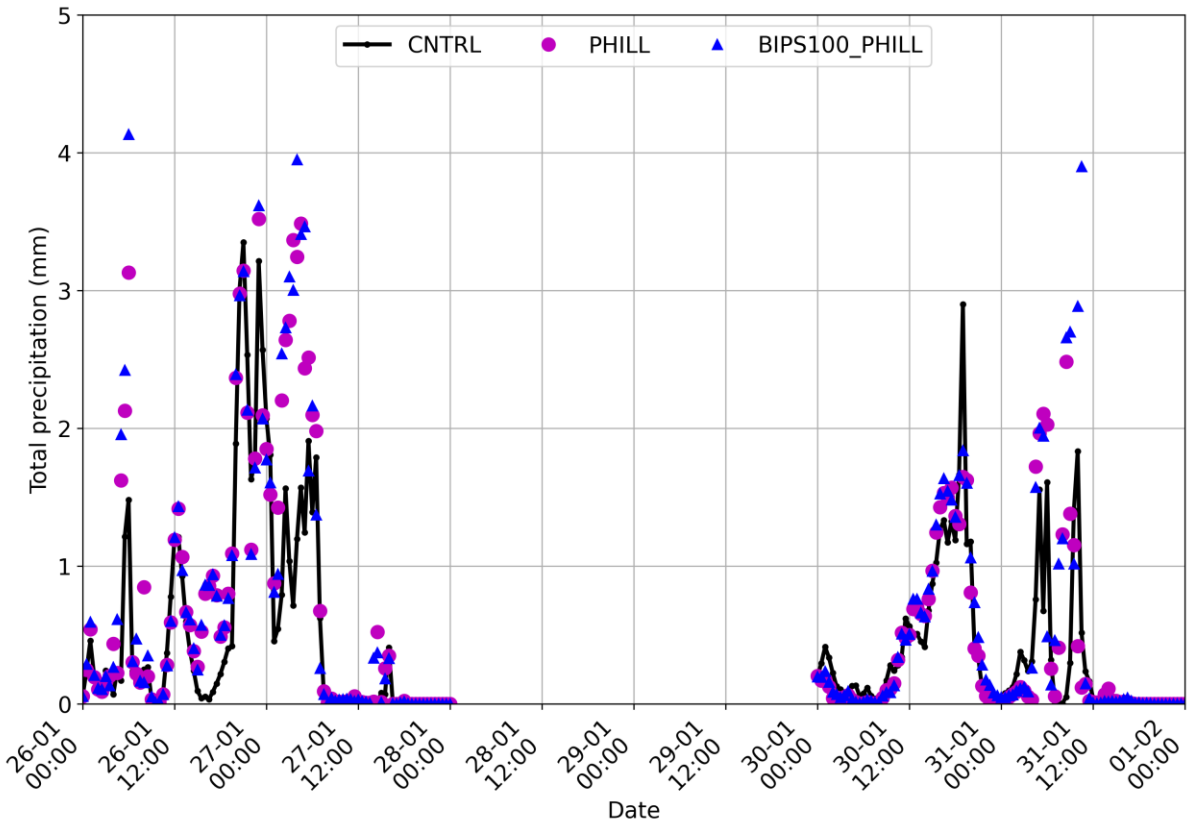

Figure S7. Total surface precipitation (rain + snow + graupel) produced by the CNTRL, PHILL and BIPS100_PHILL simulations. The latter represents the sensitivity simulation where the combined effect of blowing snow and ice-ice collisional break-up is examined.

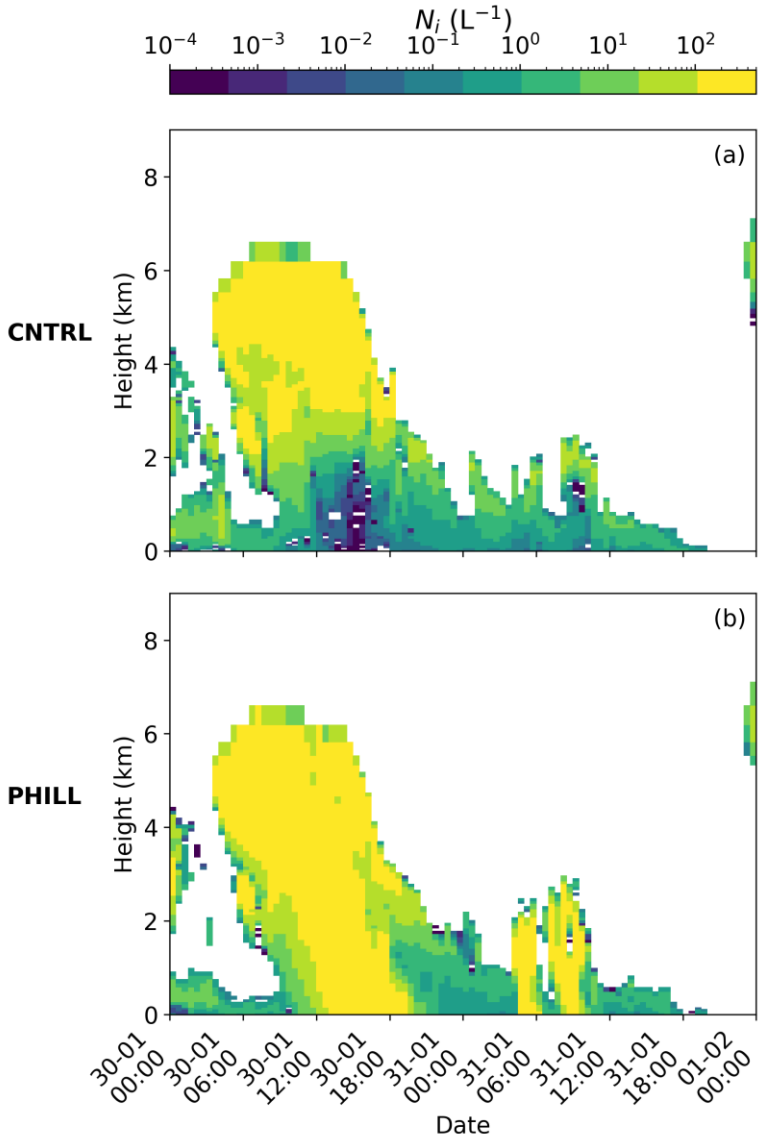

Figure S8. Time-height plots of cloud ice number concentrations (N_i) produced by (a) CNTRL and (b) PHILL simulations between 30 January and 1 February 2014. The height is given in km a.g.l.

References

Besic, N., Gehring, J., Praz, C., Figueras i Ventura, J., Grazioli, J., Gabella, M., Germann, U., and Berne, A.: Unraveling hydrometeor mixtures in polarimetric radar measurements, Atmos. Meas. Tech., 11, 4847–4866, https://doi.org/10.5194/amt-11-4847-2018, 2018.

Grazioli, J., Lloyd, G., Panziera, L., Hoyle, C. R., Connolly, P. J., Henneberger, J., and Berne, A.: Polarimetric radar and in situ observations of riming and snowfall microphysics during CLACE 2014, Atmos. Chem. Phys., 15, 13787–13802, https://doi.org/10.5194/acp-15-13787-2015, 2015.

Phillips, V. T. J., Yano, J. I. and Khain, A.: Ice multiplication by breakup in ice-ice collisions. Part I: Theoretical formulation, J. Atmos. Sci., 74(6), 1705–1719, doi:10.1175/JAS-D-16-0224.1, 2017.

Phillips, V. T. J., Patade, S., Gutierrez, J. and Bansemer, A.: Secondary ice production by fragmentation of freezing drops: Formulation and theory, J. Atmos. Sci., 75(9), 3031–3070, doi:10.1175/JAS-D-17-0190.1, 2018.

Schneebeli, M., Dawes, N., Lehning, M., and Berne, A.: High resolution vertical profiles of polarimetric X-band weather radar observables during snowfall in the Swiss Alps, J. Appl. Meteorol. Clim., 52, 378–394, doi:10.1175/JAMC-D-12-015.1, 2013.

Sullivan, S. C., Hoose, C., Kiselev, A., Leisner, T. and Nenes, A.: Initiation of secondary ice production in clouds, Atmos. Chem. Phys., 18(3), 1593–1610, doi:10.5194/acp-18-1593-2018, 2018.

Takahashi, T., Nagao, Y. and Kushiyama, Y.: Possible High Ice Particle Production during Graupel–Graupel Collisions, J. Atmos. Sci., 52, 4523–4527, 1995.